European Review for Medical and Pharmacological Sciences 2020; 24: 9453-9464

Identification of ELAVL1 gene and miRNA-139-3p involved in the aggressiveness of NSCLC

Z.-Z. NI[1,2], J.-K. HE[1], X. TANG[1], Z. TAO[2], Y. ZHANG[2], B. XIE[1]

[1]Department of Thoracic Surgery, The First Affiliated Hospital of Soochow University, Suzhou, Jiangsu, China
[2]Department of Thoracic Surgery, The First Affiliated Hospital of Wannan Medical College, Wuhu, Anhui, China

Abstract. – OBJECTIVE: Tumor metastasis remains the main cause for the cancer-associated death of human non-small-cell lung carcinoma (NSCLC). Many studies have verified that microRNAs (miRNAs) exert crucial functions in the development of NSCLC. Nevertheless, the functions of miR-139-3p in NSCLC remain unexplored.

PATIENTS AND METHODS: The quantitative Real Time-PCR (qRT-PCR) assay was applied to assess the level of miR-139-3p and ELAV like RNA binding protein 1 (ELAVL1) in NSCLC tissues and cell lines. The growth of NSCLC cell was analyzed using 3-(4,5-dimethylthiazol-2-yl)-5-(3-carboxymethoxyphenyl)-2-(4-sulfophenyl)-2H-tetrazolium (MTS) assay and colony formation assay. The migration ability and invasiveness of NSCLC cell were analyzed using wound healing and transwell invasion analysis. The expression of ELAVL1 was determined by immunoblotting assay. The growth of NSCLC cell *in vivo* was assessed using xenograft model.

RESULTS: We uncovered that miR-139-3p was down expressed in NSCLC. MiR-139-3p repressed NSCLC cell growth, migration as well as invasion *in vitro*, and suppressed the progression of NSCLC cell *in vivo*. Mechanistically, ELAVL1 was proved as a downstream target of miR-139-3p. The level of ELAVL1 was upregulated in NSCLC and inversely associated with miR-139-3p level. Immunoblotting assay suggested that ELAVL1 was negatively modulated by miR-139-3p in NSCLC cell. *In vivo*, miR-139-3p repressed NSCLC cell growth and metastasis. Several recuse assays revealed that ELAVL1 mediated the inhibitory actions of miR-139-3p on the growth and metastatic-related traits of NSCLC cell.

CONCLUSIONS: Our results indicate that miR-139-3p acts as a suppressor in modulating the aggressiveness of NSCLC *via* regulating ELAVL1.

Key Words:
NSCLC, MiR-139-3p, ELAVL1, Metastasis.

Introduction

Non-small-cell lung carcinoma (NSCLC) is one of the most common lung carcinomas and the main reason for cancer-related death worldwide. In spite of the great advances in the therapeutic strategies, the clinical outcome of patient with NSCLC is still poor due to the distant metastasis. Hence, investigations of critical factors which are involved in the metastasis of NSCLC are urgent.

Dysregulation of microRNAs (miRNAs) function as crucial factors in the development of malignancies by modulating diverse cellular processes, including cancer cell growth, migration, invasion, and angiogenesis. MiR-139-3p is downregulated in cervical carcinoma and overexpression of miR-139-3p suppresses cervical carcinoma cell proliferation and invasiveness *via* targeting NIN1 (RPN12) Binding Protein 1 Homolog (NOB1)[1]. MiR-139-3p is also found down expressed in glioma and miRNA-139-3p suppresses glioma cell metastasis *via* modulating melanoma differentiation associated gene-9 (MDA-9)/syntenin[2]. In patient with hepatocellular carcinoma (HCC), high level of miR-139-3p predicts a better prognosis[3]. Lower level of miR-139-3p is closely related with worse clinical outcomes of colorectal[4]. Nevertheless, whether miR-139-3p is involved in the progression of NSCLC remains not well illuminated.

Herein, we demonstrate that miR-139-3p is significantly down expressed in NSCLC. Functional experiments were carried out to explore the activities of miR-139-3p in the aggressive phenotypes of NSCLC cell. ELAVL1 was proved to be a downstream target gene of miR-139-3p in NSCLC and miR-139-3p inhibits the aggressiveness of NSCLC cell *via* targeting ELAVL1. This study proves that miR-139-3p suppresses

Corresponding Author: Jingkang He, MD; e-mail: 20174132168@stu.suda.edu.cn

the aggressiveness of NSCLC cell by regulating ELAVL1.

Patients and Methods

NSCLC Tissues

Tissues were collected from 46 patients in the First Affiliated Hospital of Soochow University. Written informed consents were obtained from NSCLC patients. The clinicopathological features of patients with NSCLC were summarized in Table I. This investigation was approved by the Ethics Committee of the First Affiliated Hospital of Soochow University on the basis of the Declaration of Helsinki.

Cell Lines and Transfections

Human immortalized normal bronchial epithelial cell line, BEAS-2B and NSCLC cells (H1299, H1975, HCC827, and H1650 A549) were bought from the Chinese Academy of Sciences (Shanghai, China). The cells were maintained in Dulbecco's Modified Eagle's Medium (DMEM; Thermo Fisher Scientific, Waltham, MA, USA) containing 10% fetal bovine serum (FBS; Thermo Fisher Scientific, Waltham, MA, USA) with 1% penicillin/streptomycin (Sigma-Aldrich, St. Louis, MO, USA) in a humidified incubator with 5% CO_2 at 37°C. The miRNA negative control (miR-NC), miR-139-3p mimics (miR-139-3p), miRNA control inhibitor (anti-miR-NC,) and miR-139-3p inhibitor (anti-miR-139-3p) were bought from RiboBio (Guangzhou, Guangdong, China). ELAVL1 expression plasmid (ELAVL1), specific siRNA against ELAVL1 (siELAVL1) was obtained from RiboBio (Guangzhou, Guangdong, China). Cell transfections were carried out using Lipofectamine 3000 reagent (Thermo Fisher Scientific, Waltham, MA, USA).

Real-Time Quantitative PCR (qRT-PCR) Assay

MiRVana miRNA Isolation Kit (Ambion, Austin, TX, USA) and TRIzol (Thermo Fisher Scientific, Waltham, MA, USA) were selected to extract total RNAs. Reverse transcription was performed using a TIANScript RT Kit (Tiangen Biotech, Beijing, China). The quantitative PCR was conducted using a TaqMan Human MiRNA Assay Kit (Genecopoeia, Guangzhou, Guangdong, China) and a SYBR Premix Ex Taq™ Kit (TaKaRa, Otsu, Shiga, Japan). The primers for miR-139-3p, U6, ELAVL1, and glyceraldehyde 3-phosphate dehydrogenase (GAPDH) were purchased from Realgene (Nanjing, Jiangsu, China). The relative levels of ELAVL1 or miR-13903p were calculated using the $2^{-\Delta\Delta Ct}$ method. The

Table I. Relationship between the expression of miR-139-3p and clinicopathological parameters in patients with NSCLC.

Variables		MiR-139-3p		p-value
		High (n)	Low (n)	
Age (years)				0.24
	< 50	12	16	
	> 50	10	8	
Gender				0.51
	Male	13	14	
	Female	9	10	
Tumor size				0.073
	≤ 3 cm	13	16	
	> 3 cm	9	8	
Differentiation				0.41
	High	4	8	
	Medium	5	4	
	Low	13	12	
LNM				< 0.01
	Yes	8	20	
	No	14	4	
TNM stage				< 0.01
	I	17	3	
	II+III	5	21	

Table II. Primers for qRT-PCR assay.

Primer		Primer sequence (5′-3′)
miR-139-3p	Forward	5'-TCTACAGTGCACGTGTC-3'
	Reverse	5'-GAATACCTCGGACCCTGC-3'
U6	Forward	5'-CTCGCTTCGGCAGCACA-3'
	Reverse	5'-AACGCTTCACGAATTTGCGT-3'
ELAVL1	Forward	5'-ACTGAACCGTGCTGCTGTTGG-3'
	Reverse	5'-AGGAATTGCCACTAACCGTCTTCG-3'
GAPDH	Forward	5'-GGAGCGAGATCCCTCCAAAAT-3'
	Reverse	5'-GGCTGTTGTCATACTTCTCATGG-3'

primers used in the qRT-PCR were summarized in Table II.

Proliferation Assay

3-(4,5-dimethylthiazol-2-yl)-5-(3-carboxymethoxyphenyl)-2-(4-sulfophenyl)-2H-tetrazolium (MTS; Sigma-Aldrich, St. Louis, MO, USA) assay was used to assess cell viability. The cells (3×10^3/well) were incubated into a 96-well plate. After incubation for 0, 24, 48, 72, and 96 h, 100 µl MTS (5 mg/ml) was added to 96 well plates for 4 h. 200 µl dimethyl sulfoxide (DMSO) was added into the plate. The absorbance was detected at 490 nm using a micro-plate reader (Bio-Rad, Hercules, CA, USA).

Colony Formation

The cells (1000) were plated into 6 cm dish. After 14 days, cell colonies were fixed using methanol, stained with 1% crystal violet, and counted. The visible colonies containing more than 50 cells were scored.

Transwell Invasion Assay

NSCLC cells (2×10^3) were cultured into the Matrigel (BD, Shanghai, China) coated membrane inserts of the transwell chambers (Millipore, Braunschweig, Germany). Then, the chambers were put into 6 well plates and incubated for 24 h. The invaded NSCLC cells were fixed using 4% paraformaldehyde and were stained by 1% crystal violet (Sigma-Aldrich, St. Louis, MO, USA) for 15 min. Finally, the invasive cells were counted under microscope.

Migration Analysis

The cells (2×10^3) were cultured into six-well plates and were cultured for overnight. Then, a wound was made in each well using a 200 µl tip and the wound width was measured at 0 h and 48 h.

In Situ Hybridization (ISH)

Briefly, the paraffin embedding NSCLC tissues slide was treated and hybridized with 10 pmol probe (LNA-modified and DIG labeled oligonucleotide; Exiqon, Vedbaek, Denmark) complementary to miR-139-3p. After incubation with anti-DIG-HRP fab fragments conjugated to horseradish peroxidase, and the hybridized probes were detected by incubation with 3′3-diaminobenzidine solution with nuclei counterstained with Carazzi's hematoxylin.

Animal Experiment

BALB/C nude mice were obtained from Shanghai SLAC Laboratory Animal Center of Chinese Academy of Sciences (Shanghai, China). H1975 cells (2×10^7) were subcutaneously injected into nude mice (100 µl per mouse). The length and width of tumor tissue were detected every week using Vernier caliper. Tumor volume (V) was calculated using the formula: $V = 0.5 \times (\text{length} \times \text{width}^2)$. In lung metastasis model, a total of 1×10^6 H1975 cells were suspended in 100 µl phosphate-buffered saline (PBS) and injected individually into nude mice *via* the tail veins. After 45 days, the mice were sacrificed, and lung tissue was subjected to hematoxylin-eosin (H&E) staining. Animal experiments were approved by the Animal Care and Use Committee of the First Affiliated Hospital of Soochow University.

Immunoblotting

Proteins were extracted using radio-immunoprecipitation assay (RIPA) buffer and electrophoresed using 10% sodium dodecyl sulfate polyacrylamide gel electrophoresis (SDS-PAGE). Then, proteins were transferred to polyvinylidene difluoride (PVDF) membranes (Bio-Rad, Hercules, CA, USA). Next, the membrane was incubated with ELAVL1 (1:1000, Abcam, Cambridge,

UK) or β-actin (1:1000, Santa Cruz, Dallas, Texas, USA) antibody for overnight. After that, the PVDF membrane was incubated with the second antibody for 1 h at room temperature. Finally, the target bands were detected using enhanced chemiluminescence (ECL) reagent (Beyotime Institute of Biotechnology, Haimen, China).

Luciferase Reporter Gene Assay

The wild-type (wt) and mutant type (mut) 3′-UTR of ELAVL1 was synthesized by Genecopoeia (Guangzhou, Guangdong, China). The wt or mut 3′-UTR of ELAVL1 was inserted into the downstream of pmirGLO Dual-Luciferase Vector (Genecopoeia, Guangzhou, Guangdong, China). The cells were cotransfected with ELAVL1-3′-UTR-wt and miR-139-3p or cotransfected with ELAVL1-3′-UTR-mut and miR-139-3p. After 48 h, the Luciferase activities were measured using a Luciferase Assay Kit (Genecopoeia, Guangzhou, Guangdong, China).

Statistical Analysis

All data were presented as Mean ± standard deviation (SD). All statistical analyses were performed using GraphPad Prism 7.0 (San Diego, CA, USA). The differences in the results of the two groups were calculated using either two-tailed Student's *t*-test or One-way ANOVA followed by post-hoc Dunnett's test. The relationship between ELAVL1 and miR-139-3p was measured using the Pearson's correlation analysis. $p<0.05$ was considered significant difference.

Results

MiR-139-3p Is Downregulated in NSCLC

To investigate the expression of miR-139-3p in NSCLC, miR-139-3p levels in 46 pairs of NSCLC samples and the corresponding non-cancerous samples were measured using the qRT-PCR analysis. As showed in Figure

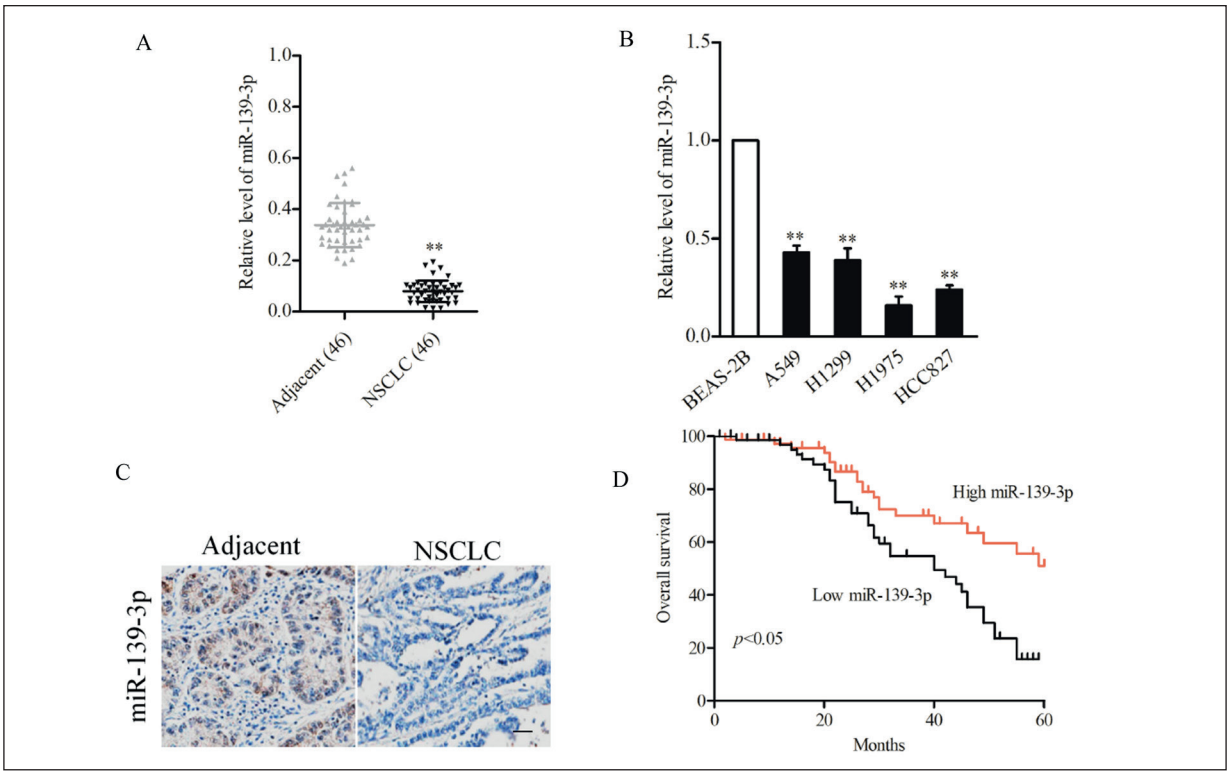

Figure 1. The expression and prognostic value of miR-139-3p in NSCLC. **A,** Levels of miR-139-3p in 46 paired human NSCLC and adjacent normal tissues were measured by qRT-PCR. **B,** qRT-PCR was performed to detect the levels of miR-139-3p in NSCLC cell lines (A549, H1299, H1975, HCC827, H1650) and BEAS-2B cells. $^{**}p<0.01$ *vs.* BEAS-2B. **C,** MiR-139-3p level in NSCLC tissue was evaluated by *in situ* hybridization (ISH) (200×, scale bar represents 200 μm). **D,** Kaplan-Meier survival analysis revealed that NSCLC patients with lower expression of miR-139-3p had poorer overall survival compared to patients with higher expression of miR-139-3p.

1A, miR-139-3p was down expressed in NSCLC compared to non-tumor tissues. Additionally, the lower expressions of miR-139-3p were observed in NSCLC cells (A549, H1299, H1975, HCC827, H1650) compared to the human immortalized normal bronchial epithelial cell line, BEAS-2B (Figure 1B). To verify our finding, we detected miR-139-3p level using ISH assay on paraffin-embedded tissue from NSCLC patients. As expected, miR-139-3p level in NSCLC tissue was lower than those in adjacent tissue (Figure 1C). Finally, Kaplan-Meier analysis indicated that patients with low level of miR-139-3p had a worse overall survival (OS) (Figure 1D). The results in Table I also show that the low level of miR-139-3p was associated with the advanced tumor-node-metastasis (TNM) stages and metastasis of NSCLC. Taken together, we demonstrate that miR-139-3p is distinctly down expressed in NSCLC.

MiR-139-3p Inhibits the Cell Viability, Migration, and Invasion of NSCLC Cell

To analyze the roles of miR-139-3p in human NSCLC, miR-139-3p mimics was transfetced into H1975 cell and A549 was transfected with anti-miR-139-3p. As showed in Figure 2A, miR-139-3p transfection significantly raised miR-139-3p level in H1975 cell and anti-miR-139-3p reduced the endogenous level of miR-139-3p in A549 cell. Next, the MTS assay indicated that the cell viability of H1975 was reduced by transfection of miR-139-3p, while the anti-miR-139-3p remarkably increased A549 cell proliferation (Figure 2B). In addition, the result of colony formation test indicated that miR-139-3p overexpression significantly decreased the colony formation capacity of H1975 cell, while anti-miR-139-3p increased the colony-formation ability of A549 cell (Figure 2C). Then, the migration assay indicated that the overexpression of miR-139-3p evidently reduced the percentage of H1975 cell migration. On the contrary, the migration of A549 cell was significantly raised by anti-miR-139-3p (Figure 2D). Furthermore, the invasion assay implied that miR-139-3p strikingly restrained the invasion ability of H1975 cell, while the invasion capacity of A549 cell was significantly increased by anti-miR-139-3p (Figure 2E). Altogether, we prove that upregulation of miR-139-3p restrains NSCLC cell growth and metastatic abilities *in vitro*.

MiR-139-3p Represses NSCLC Cell Growth and Metastasis in Vivo

We next analyzed the impacts of miR-139-5p on the progression of NSCLC cell *in vivo*, miR-139-3p transfected H1975 cells were implanted into nude mice. As shown in Figure 3A-3B, the tumor growth curve and tumor weight were both inhibited in nude mice that was inoculated with miR-139-3p transfected H1975 cell. Then, the level of miR-139-3p in tumor tissue was confirmed using qRT-PCR assay and we observed that the level of miR-139-3p in mice that was inoculated with miR-139-3p transfected H1975 cell was higher compared to that in the miR-NC group (Figure 3C). Additionally, the results of immunohistochemistry (IHC) assay suggested that the percentage of ELAVL1 positive staining cells in mice that were injected with miR-139-3p transfected H1975 cell was significantly reduced than that in control group (Figure 3D). Finally, miR-139-3p transfected H1975 cells were injected into mice *via* the tail vein to reveal the influence of miR-139-5p on H1975 cell metastasis *in vivo*. As shown in Figure 3E-3F, the number of metastatic nodules in mice that were injected with miR-139-3p transfected H1975 cell was markedly less than that in control group. All these findings indicate that miR-139-3p represses the growth and metastatic capacity of NSCLC cell *in vivo*.

ELAVL1 Is A Target of MiR-139-3p

To illuminate the mechanisms behind the function of miR-139-3p in NSCLC, "TargetScan", and "miRTarBase" and "miRDB" online platform were selected to find the targets of miR-139-3p. We screened five target genes using the three prediction databases, including fructosamine 3 kinase (FN3K), ubiquitin conjugating enzyme E2 G1 (UBE2G1), mitochondrial elongation factor 1 (MIEF1), coiled-coil domain containing 71 like (CCDC71L), and ELAVL1 (Figure 4A). Nevertheless, only ELAVL1 level was modulated by miR-139-3p (Figure 4B-4C). Next, qRT-PCR assay indicated that ELAVL1 was overexpressed in NSCLC samples when compared with that in the normal tissues (Figure 4D). Consistently, IHC staining using ELAVL1 antibody indicated ELAVL1 was markedly unregulated in NSCLC tissue (Figure 4E). OF note, miR-139-3p level was inversely associated with the expression of ELAVL1 gene in NSCLC tissues (Figure 4F). Finally, Luciferase reporter

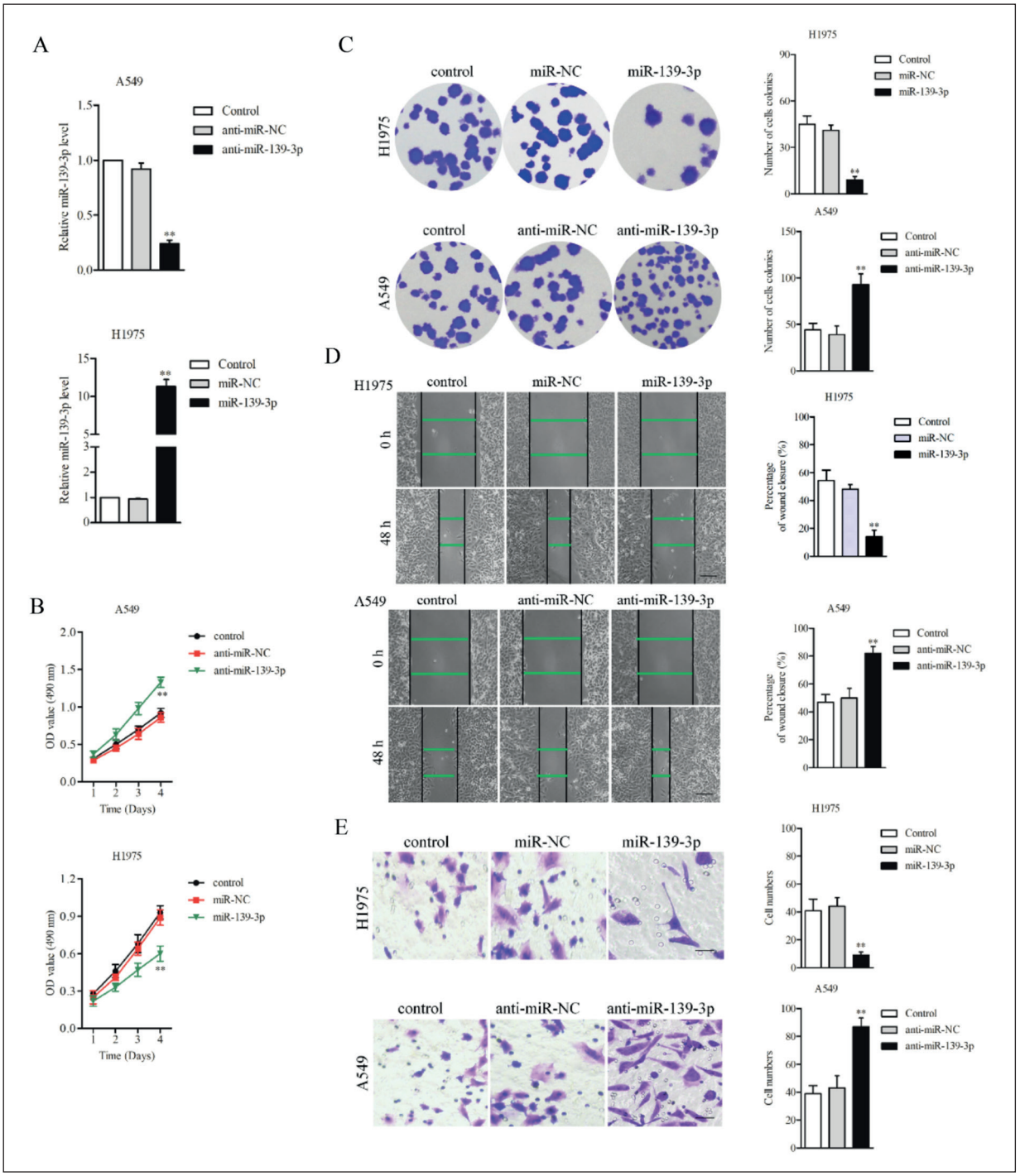

Figure 2. MiR-139-3p inhibits NSCLC cell proliferation and motility *in vitro*. **A,** Level of miR-139-3p in H1975 transfected miR-139-3p mimics and A549 cell transfected with miR-139-3p inhibitor (anti-miR-139-3p) was detected using qRT-PCR assay. **B,** MTS assay revealed that miR-139-3p decreased the viability of H1975 and anti-miR-139-3p increased the proliferation of A549 cell. **C,** MiR-139-3p mimics inhibited the colony formation of H1975 cell and anti-miR-139-3p raised the colony formation of A549 cell (200×, scale bar represents 200 μm). **D,** MiR-139-3p restrained the migration of H1975 and anti-miR-139-3p enhanced the migration of A549 cell. **E,** MiR-139-3p restrained the invasion of H1975 and anti-miR-139-3p enhanced the invasion of A549 cell (200×, scale bar represents 200 μm). $^{**}p<0.01$ *vs.* control.

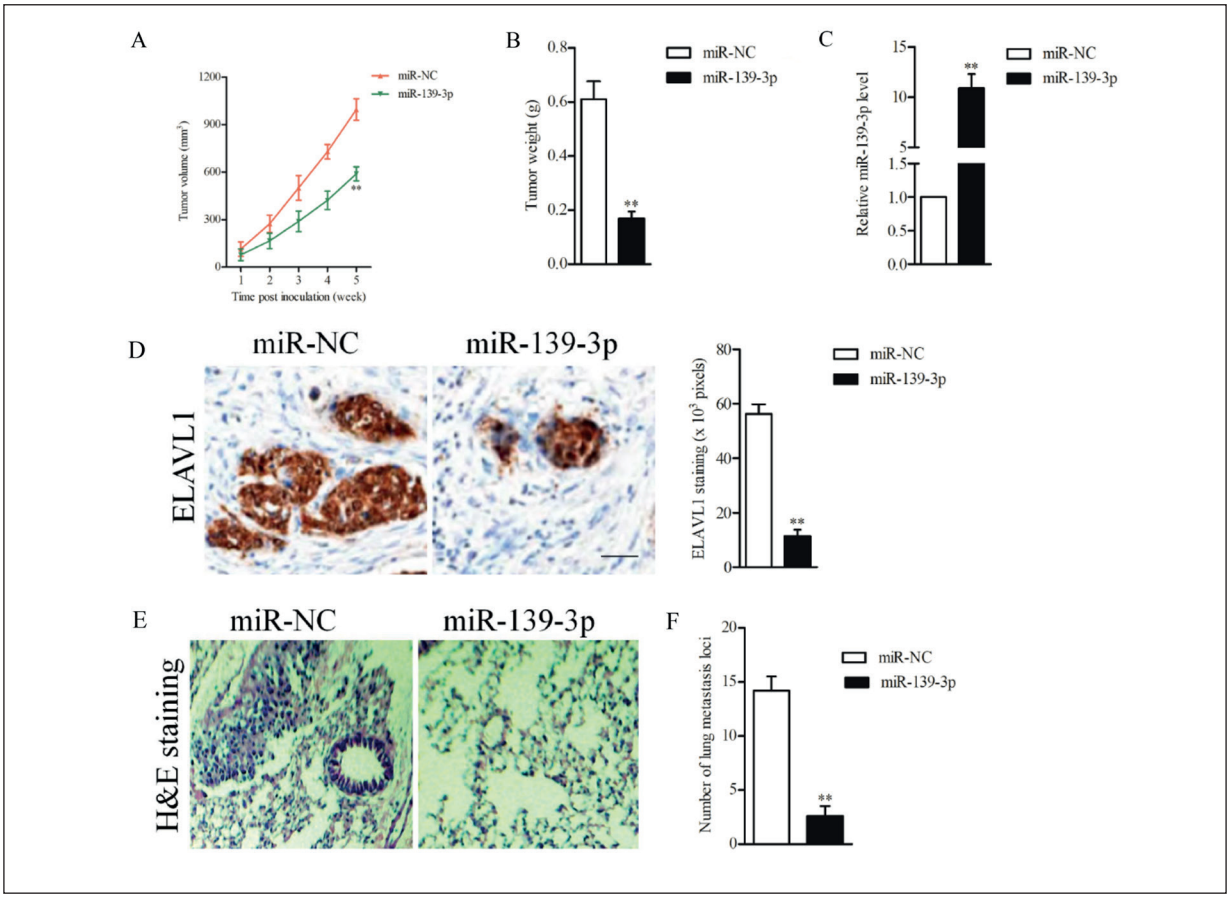

Figure 3. MiR-139-3p restrains the growth and metastasis of NSCLC cell *in vivo*. **A,** MiR-139-3p transfected H1975 cells were subcutaneously implanted into nude mice. The tumor growth curves indicated that miR-139-3p suppressed the growth of NSCLC cells. **B,** Subcutaneous tumors were harvested and weighted at the 35 days after implantation. **C,** Tumor tissues were subjected to qRT-PCR for the expression of miR-139-3p. **D,** Immunostaining of ELAVL1 using xenograft tissues from miR-139-3p silencing group and control group (200×, scale bar represents 200 μm). **E,** H&E staining of metastatic lung nodules in miR-139-3p silencing group and control group. **F,** Quantitative analysis of lung micrometastatic foci in lung tissue. $^{**}p<0.01$ *vs.* miR-NC.

assay was carried out and we observed that miR-139-3p suppressed the Luciferase activity in NSCLC cell which was transfected with wt-3′-UTR of ELAVL1 but not mut-3′-UTR of ELAVL1 (Figure 4G). These data indicate that ELAVL1 is a target of miR-139-3p.

ELAVL1 Rescued the Suppressive Effects of MiR-139-3p on NSCLC Cell

To explore whether ELAVL1 participates in the suppressive actions of miR-139-3p in NSCLC, rescue experiments were carried out. H1975 cell was transfected with miR-139-3p alone or cotransfected with ELAVL1 and miR-139-3p. As shown in Figure 5A, ELAVL1 expression plasmid significantly abolished the suppressive impact of miR-139-3p on ELAVL1 level in H1975 cell. Then, the MTS and colony formation assay implied that miR-1393p suppressed the proliferation of H1975 cells, and ELAVL1 expression reversed the inhibitory effect of miR-139-3p on H1975 cell growth and colony formation (Figure 5B-5C). Next, migration and transwell invasion assays demonstrated that restoration of ELAVL1 abolished the suppressive impacts of miR-139-3p on H1975 cell (Figure 5D-5E). Our data demonstrate that ELAVL1 is a functional target gene of miR-139-3p.

ELAVL1 Silencing Inhibits the Aggressiveness of NSCLC in the Presence of Anti-miR-139-3p

To confirm that miR-139-3p inhibits the aggressiveness of NSCLC cell by targeting ELAVL1,

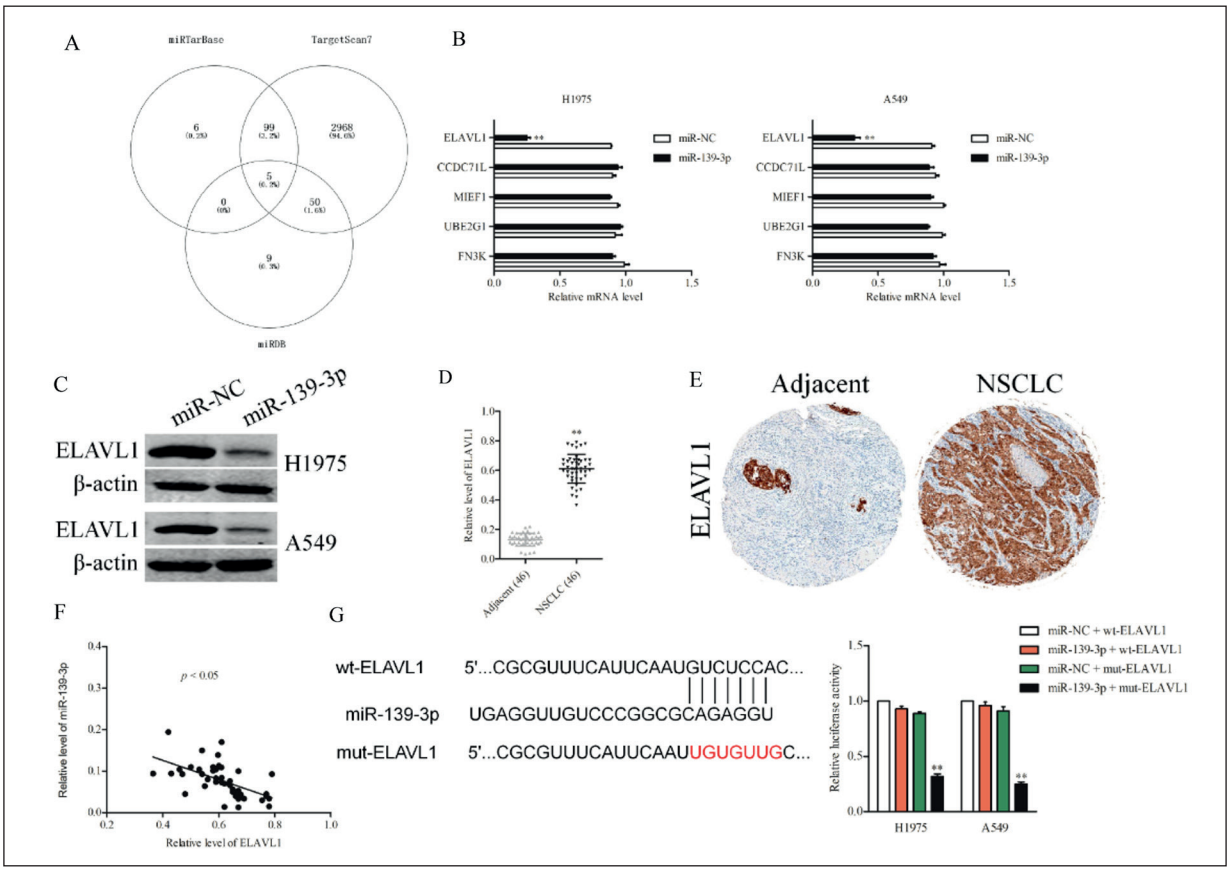

Figure 4. ELAVL1 is a target of miR-139-3p in NSCLC. **A,** Venn diagram depicting the overlap between the predicted gene targets for miR-139-3p. **B,** mRNA levels of potential targets of miR-139-3p were detected using qRT-PCR. $^{**}p<0.01$ *vs.* miR-NC. **C,** Western blotting showed that ELAVL1 could be significantly negatively regulated by miR-139-3p at the protein level in NSCLC cell. **D,** The mRNA levels of ELAVL1 in 46 paired NSCLC and adjacent normal tissues. **E,** Levels of ELAVL1 in NSCLC and adjacent normal tissue were measured using IHC staining assay. **F,** Pearson correlation analysis revealed that there existed an inverse correlation between the mRNA level of ELAVL1 and miR-139-3p level in NSCLC tissue. **G,** Putative miR-139-3p binding site in the 3′-UTR of ELAVL1 was predicted by TargetScan. The mutant binging site was generated in the complementary site for the seed region of miR-139-3p. Luciferase reporter gene assay showed that miR-139-3p overexpression suppressed the Luciferase activity of vector carrying wt-3′-UTR of ELAVL1 but not of the mut-3′UTR in NSCLC cell. $^{**}p<0.01$ *vs.* miR-NC + wt-ELAVL1.

A549 cell was transfected with anti-miR-139-3p or cotransfected with siELAVL1 and anti-miR-139-3p. As shown in Figure 6A, siELAVL1 significantly abolished the promoting impact of anti-miR-139-3p on ELAVL1 level in A549 cell. Then, the MTS and colony formation assays implied that anti-miR-1393p enhanced the proliferation of A549 cell, and siELAVL1 impaired the promoting effects of anti-miR-139-3p on A549 cell growth and colony formation (Figure 6B-6C). Next, the migration and transwell invasion assays demonstrated that downregulation of ELAVL1 weakened the promoting impacts of anti-miR-139-3p on A549 cell migration and invasion (Figure 6D-6E). Our results demonstrate that miR-139-3p inhibits the aggressiveness of NSCLC cell by targeting ELAVL1.

Discussion

An increasing number of reports[5-7] verify that miRNAs exert vital functions in the regulation of human NSCLC tumorigenesis and metastasis. Hence, investigations of suppressive or oncogenic miRNAs, which are related with NSCLC development, are useful to explore potential therapeutic targets for NSCLC. In the present research, miR-139-3p was found down expressed in NSCLC cells and clinical tissues. Moreover, the low

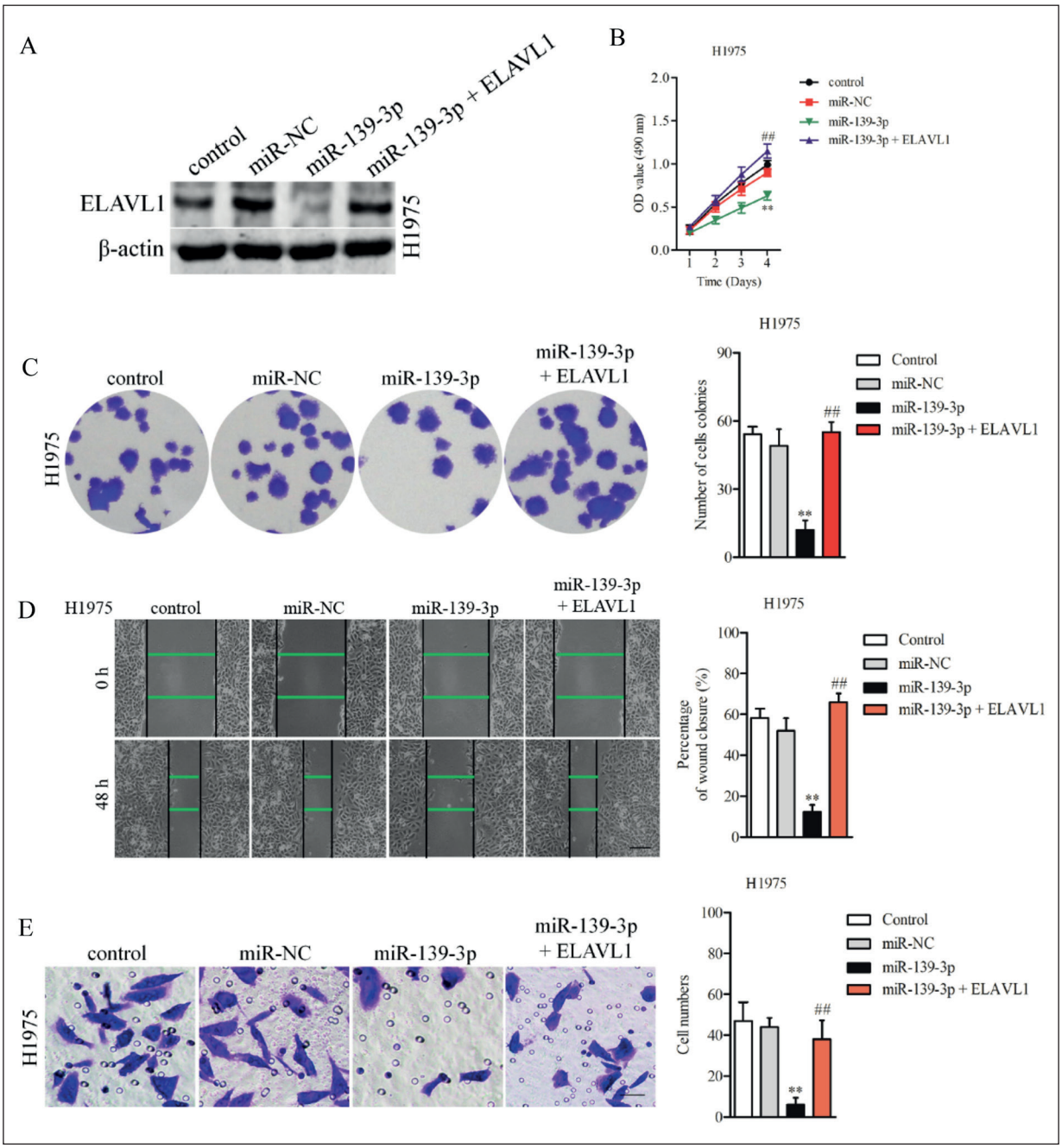

Figure 5. ELAVL1 mediates the effects of miR-139-3p on NSCLC cell. **A,** Transfection efficiency was confirmed by western blotting. **B,** MTS assay revealed that miR-139-3p decreased the viability of H1975 cell, which partially reversed by ELAVL1 re-expression. **C,** Colony formation assay revealed that miR-139-3p decreased the viability of H1975 cell, which partially reversed by ELAVL1 re-expression (200×, scale bar represents 200 μm). **D,** Wound healing assay revealed that ELAVL1 re-expression reversed the suppressive effect of miR-139-3p on migration of NSCLC cells. **E,** Transwell invasion assays showed that and ELAVL1 reversed the inhibitory effect of miR-139-3p on mobility of NSCLC cell (200×, scale bar represents 200 μm). $^{**}p<0.01$ *vs.* control, $^{\#\#}p<0.01$ *vs.* miR-139-3p.

expression of miR-139-3p was closely associated with poor prognosis of patients with NSCLC.

Recently, the functional roles of miR-139-3p in malignancies have been proposed[4,8,9]. To date, the precise roles of miR-139-3p in the malignant progression of NSCLC remains not well explored. Here, we proved that miR-139-3p suppressed the growth and metastatic capacities

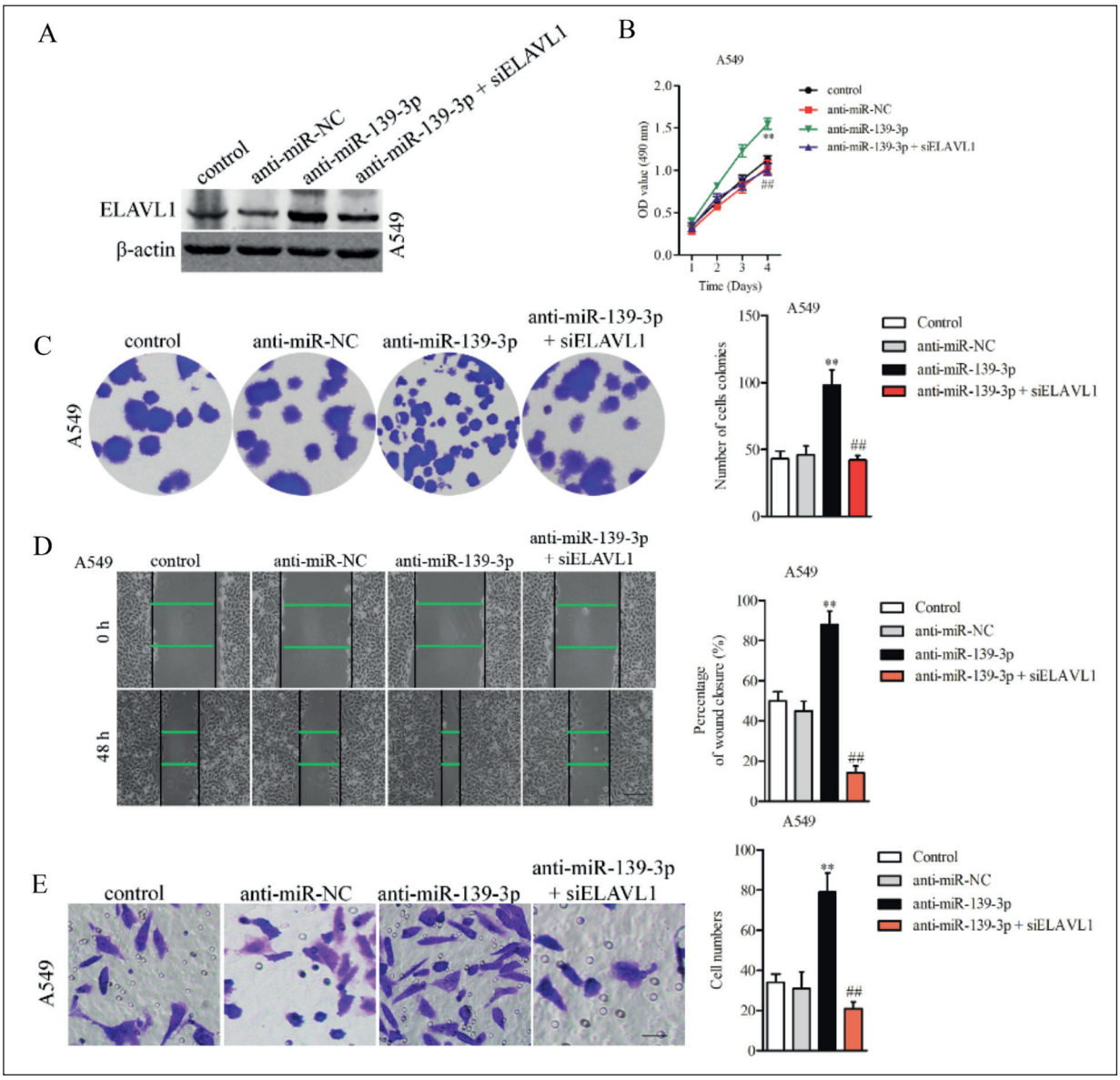

Figure 6. ELAVL1 silencing inhibits the aggressiveness of NSCLC in the presence of anti-miR-139-3p. **A,** Transfection efficiency was confirmed by Western blotting. **B,** MTS assay revealed that anti-miR-139-3p increased the viability of H1975 cell, which partially reversed by siELAVL1. **C,** Colony formation assay revealed that anti-miR-139-3p increased the growth of H1975 cell, which partially reversed by siELAVL1 (200×, scale bar represents 200 μm). **D,** Wound healing assays showed that siELAVL1 weakened the mobility of NSCLC cells in the presence anti-miR-139-3p. **E,** Transwell invasion assays showed that siELAVL1 weakened the invasion of NSCLC cell in the presence anti-miR-139-3p (200×, scale bar represents 200 μm). $^{**}p<0.01$ *vs.* control, $^{\#\#}p<0.01$ *vs.* anti-miR-139-3p.

of NSCLC cell *in vitro* using gain-of-function and loss-of-function experiments. Tian et al[2] proved that miRNA-139-3p restrains the proliferation and metastatic-related traits of human glioma cell by modulating MDA-9/syntenin. High miR-139-3p expression also predicts a better prognosis for hepatocellular carcinoma[3]. In cervical cancer, miR-139-3p induces apoptosis and suppresses the metastasis of cancer cell *via* modulating NOB1[1]. Downregulated miR-139-3p enhances bladder cancer cell migration and invasion by targeting matrix metallopeptidase

11 (MMP11)[8]. We also proved that miR-139-3p markedly inhibited NSCLC cell growth and metastatic ability *in vivo*. Overall, our observations suggest that miR-139-3p serves as a suppressive miRNA in NSCLC.

In this research, we further demonstrated that ELAVL1 was a downstream target of miR-139-3p in NSCLC. ELAVL1, which belongs to a member of the Hu family of RNA-binding protein, plays critical roles in several cancers[9-12]. Previous investigations[13,14] have indicated that ELAVL1 is overexpressed in lung cancer and regulates the proliferation of NSCCL cell and survival of patients. In addition, miR-19b non-canonical binding is directed by ELAVL1 and confers chemosensitivity through the regulation of P-glycoprotein in breast carcinoma[15]. In this study, we also observed that the expression of ELAVL1 was markedly inhibited in miR-139-3p overexpressing NSCLC cell. Next, Luciferase reporter gene assay demonstrated that ELAVL1 was a target gene of miR-139-3p. Notably, we observed that miR-139-3p was inversely associated with the level of ELAVL1 in clinical NSCLC samples. Finally, restoration of ELAVL1 reversed the suppressive functions of miR-139-3p in NSCLC cell. These findings indicated that ELAVL1 played a crucial role in miR-139-3p-induced NSCLC progression. Altogether, we proved that miR-139-3p was down expressed in NSCLC. In addition, miR-139-3p restrained the growth and aggressive phenotypes of NSCLC cell by regulating ELAVL1.

Conclusions

We illuminate that miR-139-3p is down expressed in NSCLC and its low level is correlated with worse prognosis of patient with NSCLC. Functionally, miR-139-3p represses the growth and metastatic traits of NSCLC cell *in vitro* and suppresses the growth and metastatic ability of NSCLC cell *in vivo*. In addition, ELAVL1 is authenticated as a functional downstream target of miR-139-3p and mediates the inhibitory impacts of miR-139-3p on the aggressiveness of NSCLC cell.

Conflict of Interest

The Authors declare that they have no conflict of interests.

References

1) Huang P, Xi J, Liu S. MiR-139-3p induces cell apoptosis and inhibits metastasis of cervical cancer by targeting NOB1. Biomed Pharmacother 2016; 83: 850-856.
2) Tian W, Wu W, Li X, Rui X, Wu Y. MiRNA-139-3p inhibits the proliferation, invasion, and migration of human glioma cells by targeting MDA-9/syntenin. Biochem Biophys Res Commun 2019; 508: 295-301.
3) Zhu Y, Zhou C, He Q. High miR-139-3p expression predicts a better prognosis for hepatocellular carcinoma: a pooled analysis. J Int Med Res 2019; 47: 383-390.
v4) Liu X, Duan B, Dong Y, He C, Zhou H, Sheng H, Gao H, Zhang X. MicroRNA-139-3p indicates a poor prognosis of colon cancer. Int J Clin Exp Pathol 2014; 7: 8046-8052.
5) Wang R, Chen X, Xu T, Xia R, Han L, Chen W, De W, Shu Y. MiR-326 regulates cell proliferation and migration in lung cancer by targeting phox2a and is regulated by HOTAIR. Am J Cancer Res 2016; 6: 173-186.
6) Gao Y, Fan X, Li W, Ping W, Deng Y, Fu X. miR-138-5p reverses gefitinib resistance in non-small cell lung cancer cells via negatively regulating G protein-coupled receptor 124. Biochem Biophys Res Commun 2014; 446: 179-186.
7) Liu R, Zhang YS, Zhang S, Cheng ZM, Yu JL, Zhou S, Song J. MiR-126-3p suppresses the growth, migration and invasion of NSCLC via targeting CCR1. Eur Rev Med Pharmacol Sci 2019; 23: 679-689.
8) Yonemori M, Seki N, Yoshino H, Matsushita R, Miyamoto K, Nakagawa M, Enokida H. Dual tumor-suppressors miR-139-5p and miR-139-3p targeting matrix metalloprotease 11 in bladder cancer. Cancer Sci 2016; 107: 1233-1242.
9) Gu C, Zhang M, Sun W, Dong C. Upregulation of miR-324-5p inhibits proliferation and invasion of colorectal cancer cells by targeting ELAVL1. Oncol Res 2019; 27: 515-524.
10) Zhang F, Cai Z, Lv H, Li W, Liang M, Wei X, Zhou F. Multiple functions of HuR in urinary tumors. J Cancer Res Clin Oncol 2019; 145: 11-18.
11) Chou SD, Murshid A, Eguchi T, Gong J, Calderwood SK. HSF1 regulation of beta-catenin in mammary cancer cells through control of HuR/elavL1 expression. Oncogene 2015; 34: 2178-2188.
12) Melling N, Taskin B, Hube-Magg C, Kluth M, Minner S, Koop C, Grob T, Graefen M, Heinzer H, Tsourlakis MC, Izbicki J, Wittmer C, Huland H, Simon R, Wilczak W, Sauter G, Steurer S, Schlomm T, Krech T. Cytoplasmic accumulation of ELAVL1 is an independent predictor of biochemical recurrence associated with genomic instability in prostate cancer. Prostate 2016; 76: 259-272.
13) Doller A, Pfeilschifter J, Eberhardt W. Signalling pathways regulating nucleo-cytoplasmic shuttling

of the mRNA-binding protein HuR. Cell Signal 2008; 20: 2165-2173.

14) Blaxall BC, Dwyer-Nield LD, Bauer AK, Bohlmeyer TJ, Malkinson AM, Port JD. Differential expression and localization of the mRNA binding proteins, AU-rich element mRNA binding protein (AUF1) and Hu antigen R (HuR), in neoplastic lung tissue. Mol Carcinog 2000; 28: 76-83.

15) Thorne JL, Battaglia S, Baxter DE, Hayes JL, Hutchinson SA, Jana S, Millican-Slater RA, Smith L, Teske MC, Wastall LM, Hughes TA. MiR-19b non-canonical binding is directed by HuR and confers chemosensitivity through regulation of P-glycoprotein in breast cancer. Biochim Biophys Acta Gene Regul Mech 2018; 1861: 996-1006.